- Technical Paper -

FLEXURAL BEHAVIOR OF EXTERNALLY PRESTRESSED CONCRETE BEAMS BY CONSIDERING LOADING APPLICATION

Chunyakom SIVALEEPUNTH[*1], Junichiro NIWA[*2], Satoshi TAMURA[*3] and Yuzuru HAMADA[*4]

ABSTRACT

The aim of this study is to investigate the flexural behavior of externally prestressed concrete (PC) beams by varying the geometry of loading application. This paper describes the experimental investigation conducted to clarify the flexural behavior of such beams. The experimental results are also compared with the nonlinear finite element method (FEM) and the simplified methods in the current codes. It is found that the experimental results agree well with the analytical predictions, but they do not satisfy with most using simplified methods.
Keywords: prestressed concrete, flexural strength, tendon strain, unbonded prestressing, loading application

1. INTRODUCTION

Externally prestressed concrete (PC) members, in which the prestressing tendons are placed outside of the concrete section and transfer the load to the concrete through end anchorages or deviators, have attracted the engineer's attention. They provide the efficiency in the new construction of segmental bridge box girders and in the repairing of existing structures which providing the simplicity during the construction and the maintenance periods. With the widely use of external tendons in PC structures, an examination of the design and analysis of such structures is needed.

The analysis of externally PC beams (i.e. beams prestressed with unbonded tendon) offers the additional level of difficulty in comparison to the analysis of conventional PC beams (i.e. beams prestressed with bonded tendons). That is the stress increase in the external tendons, which is depending on the entire deformation of the member and variations of eccentricity of external tendons

under the additional load. It is commonly referred as the second-order effects. The stress increase in the external tendon cannot be determined from the conventional strain compatibility as in the case of bonded tendons, but it must be determined from the analysis of deformation of the entire structure.

In this study, the experimental investigations of PC beams with external tendons were conducted by varying the geometry of loading application. This paper addressed the suitable analytical model in nonlinear finite element method (FEM) for evaluating the flexural strength of externally PC beams by varying the geometry of loading application. The study compared the experimental results with the prediction equations recommended by ACI318-99 [1] and AASHTO LRFD [2] design codes. However this study did not compare the results with JPCEA [3], since the stress increment in unbonded tendons in JPCEA code is set as a constant value as 200 N/mm^2. Therefore, a modification of simplified method used for a design guideline is needed.

---

*1   Graduate School of Civil Engineering, Tokyo Institute of Technology, JCI Member
*2   Prof., Dept. of Civil Engineering, Tokyo Institute of Technology, Dr. E., JCI Member
*3   Research Engineer, Research and Development Center, DPS Bridge Works Co., Ltd., JCI Member
*4   Manager, Research and Development Center, DPS Bridge Works Co., Ltd., Dr. E., JCI Member

2. TEST PROGRAMS

The test specimens consisted of three prototype PC beams with external tendons, with the same total length at 3.3 m, cross section dimensions and reinforcement details as shown in Fig. 1. The specimens were named as T3_L00_S15, T3_L05_S15 and T3_L10_S15 as shown in Table 1. The plastic region length is considered to mainly govern the stress increment in external tendons, which is related to the geometry of loading application [4]. Therefore the main parameter in this study is the geometry of loading applications whether it is one-point loading or two-point loading with the loading distance equal to 500 mm or 1000 mm.

2.1 Materials
(1) Reinforcements

In all specimens, the internal longitudinal tensile reinforcement consisted of two deformed steel bars with nominal diameter of 16 mm and four deformed steel bars are for longitudinal compressive reinforcement with nominal diameter of 6 mm. Their average yield strength is 365 N/mm^2 and 307.4 N/mm^2, and average tensile strength is 534.1 N/mm^2 and 482.1 N/mm^2, respectively. Transverse reinforcement consisting of deformed steel stirrups with a nominal diameter of 6 mm and with yield strength of 307.4 N/mm^2 was provided throughout the length of the beams.

(2) Concrete

The concrete has a mix proportion as summarized in Table 2. The water cement ratio was 0.40 and the design cylindrical compressive strength of concrete was 55 N/mm^2 at 28 days. The actual strength of concrete in each batch of casting was measured. The beams were covered with moistened cloths and the formwork was removed 4 or 5 days after casting. Moist-curing was continued until the 21st day after casting.

Table 1 Detail of test beams

Beams	Effective span length, L [mm]	Loading distance, L_a [mm]	Deviator spacing, S_d [mm]	Depth of tendon, d_{ps} [mm]	Effective prestress, f_{pe} [N/mm^2]	Area of internal steel bars, A_s [mm^2]	Area of external tendon, A_{ps} [mm^2]
T3_L00_S15		0			956.9		
T3_L05_S15	3000	500	1500	200	918.7	397.2	281.4
T3_L10_S15		1000			913.5		

Table 2 Mix proportion of casting concrete

G_{max} [mm]	W/C [%]	s/a [%]	UNIT: [kg/m^3]				
			W[*1]	C[*2]	S[*3]	G[*4]	SP[*5] [%]
20	40.0	54.0	168	425	911	792	0.56

*1 Water
*2 Ordinary portland cement, specific gravity = 3.16
*3 Fine aggregate, specific gravity = 2.60, F.M. = 2.63
*4 Coarse aggregate, specific gravity = 2.64, F.M. = 6.89
*5 Superplasticizer, specific gravity = 1.44
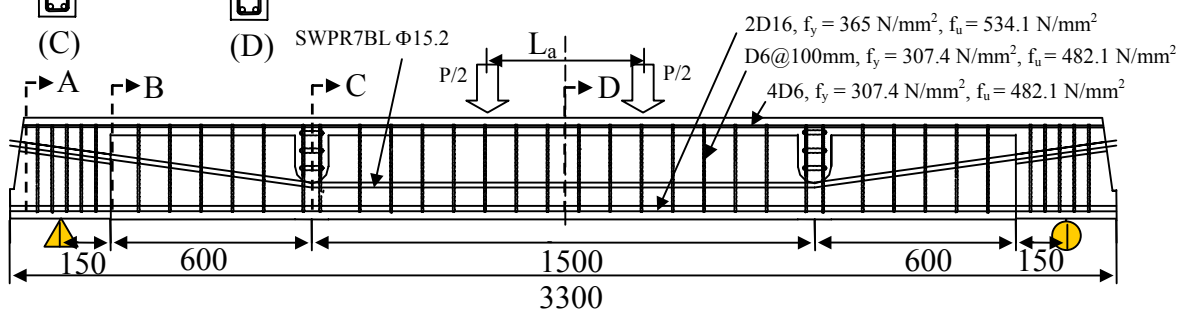
Fig.1 Dimensions and steel layout of beam specimens

(3) External tendons

Two straight 7-wire prestressing tendons with a nominal diameter of 15.2 mm were prepared for each specimen as external tendons. The yield strength f_{py}, the tensile strength f_{pu} and the modulus of elasticity of tendons E_{ps} were 1695 N/mm², 1905 N/mm² and 193.1 kN/mm², respectively.

2.2 Experimental Setup

After the beams were cured more than 28 days, they were prestressed using symmetrically arranged external tendons on both sides of the section of externally PC beams deviated at one-third of the beams by two monolithic concrete deviators and anchored at the ends of the beams. Prior to this, the friction-reducing pads, i.e. two Teflon sheets (0.05 mm thickness) sandwiching silicon grease, were inserted between the beam specimen and the support plates, and also between the tendons and deviators for reducing the friction. In order to keep a balance of prestressing in both tendons, each tendon was prestressed alternatively by an increment of 10 kN. Three electrical strain gauges were placed on each tendon on three of seven wires of the tendon at the same section at the midspan of the beam. The strain of the prestressing tendon was taken as the average value of the three measured strain locations.

All beams had draped tendon profiles, with a depth of 200 mm at the midspan section. The tendons were stressed to about $0.55f_{pu}$ that is effective prestress, f_{pe} as shown in Table 1. Each beam was instrumented to measure midspan deflections, tendon level, crack width, and strains of concrete, steel and tendon. The beams were simply supported over a span of 3 m and loaded in one-point loading at the midspan for the specimen T3_L00_S15 and two-point loading for specimens T3_L05_S15 and T3_L10_S15.

3. FEM ANALYSIS

The nonlinear FEM using DIANA system has been conducted to examine the flexural behavior of externally PC beams. Because of the symmetric property of a beam, a half of specimen with an 8-node quadrilateral isoparametric plane stress element in a two dimensional configuration is modeled as shown in Fig. 2. In Fig. 2, the interface element used at the deviator is also shown. The friction between tendon and deviator is neglected. The stiffness in n-axis, D_n is set to be infinity in order to fix tendon with the deviator in n-axis. For t-axis, the stiffness, D_t is set to be zero due to the frictionless between deviator and tendon.

In the analysis, the smeared crack model is adopted as the crack model to concrete elements. Figure 3 shows the constitutive model of concrete under compressive stress states. The compressive model of concrete is assumed to behave as a second-degree parabola up to its peak. A linear descending branch considering the
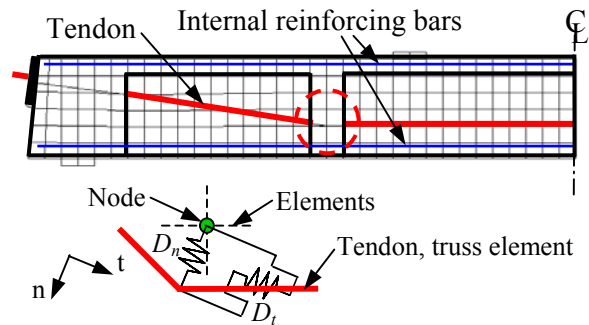
Fig. 2 Finite element analytical model and interface element at deviator

$$\sigma = f_c' \left\{ \frac{2\varepsilon}{\varepsilon_p} - \left(\frac{\varepsilon}{\varepsilon_p} \right)^2 \right\}; \quad \varepsilon_p = 2.7 \times 10^{-4} \cdot \sqrt[4]{145.04 \cdot f_c'}$$

$$\sigma = \frac{\varepsilon - \varepsilon_u}{\varepsilon_u - \varepsilon_p}$$

$$\varepsilon_u = \frac{2G_{fc}}{f_c' \cdot L_{elm}} - \varepsilon_0$$

$$G_{Fc} = 8.8\sqrt{f_c'}$$

$$\varepsilon_0 = \varepsilon_p / 2$$

L_{elm}: element size

Fig. 3 Constitutive model of concrete under compressive stress states

E_c : Modulus of elasticity
f_t : Tensile strength

Hordijk's model
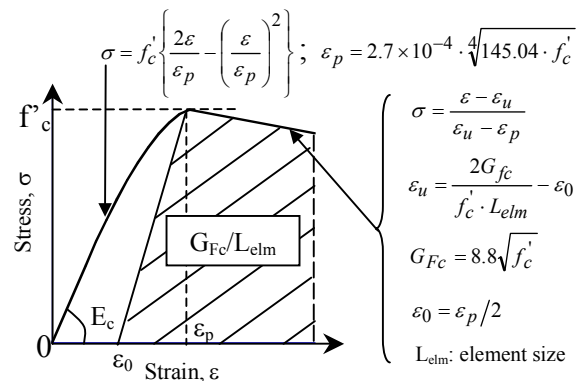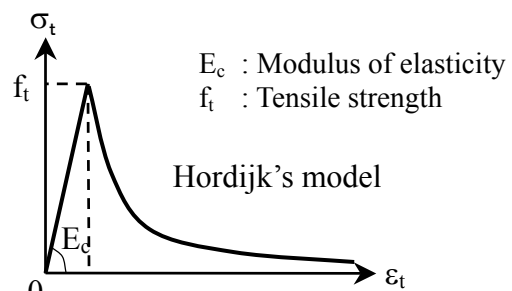
Fig. 4 Tension softening model

compressive fracture energy, G_{Fc} in terms of the element size proposed by Nakamura, H., et al. [5] is also applied. The compressive fracture energy is considered in the shaded area in Fig. 3.

After cracking, the tension softening model proposed by Hordijk [6] is utilized as the concrete constitutive model under tension as illustrated in Fig. 4. The yield conditions of Rankine are applied as the tension failure criteria. Two-node truss elements are applied as the tendon elements. The reinforcement elements are modeled to have the perfect bond with concrete. The bilinear elasto-plastic model of steel is adopted for the longitudinal reinforcement and prestressing tendons. As the first step of the analysis, the prestressing force is applied by using the incorporated prestressing command in DIANA system.

4. RESULTS AND DISCUSSION

4.1 Cracking Behavior

The crack patterns of all specimens were similar except for one-point loading beam T3_L00_S15 as demonstrated in Fig 5. Flexural cracks were firstly observed in the flexural span for two-point loading beams T3_L05_S15 and T3_L10_S15 while the initial crack occurred at the midspan of one-point loading beam T3_L00_S15. As the load increased, several simultaneous cracks were mainly developed inside the flexural span for the case of two-point loading beams. Flexural shear cracks also appeared in the shear span of the beams. However, only one crack or occasionally two cracks out of the several cracks formed were observed to increase significantly in width and to propagate upward to the compression zone of the beam. The loading was continued until the crushing of concrete occurred in the flexural span at the compression zone.

4.2 Load-deflection Response

The response of applied load versus deflection of beams is illustrated in Fig. 6. All beams showed the similar behavior. The summary of the measured specimens resistances from the cracking to the ultimate

load together with the midspan deformation and tendon level at the ultimate stage are summarized in Table 3. At the beginning, the beams behaved as the linear elastic uncracked until the first crack occurred that reduced the beam stiffness. It is found that the flexural cracks occurred at approximately 50 percent of the ultimate load. After the crack stabilized, the deflection increased linearly with the applied load until the internal reinforcing bars started to yield. After the yield of internal reinforcing bars, the deflection increased nonlinearly with the slight increase in load until the ultimate resistance. At ultimate, the beams showed
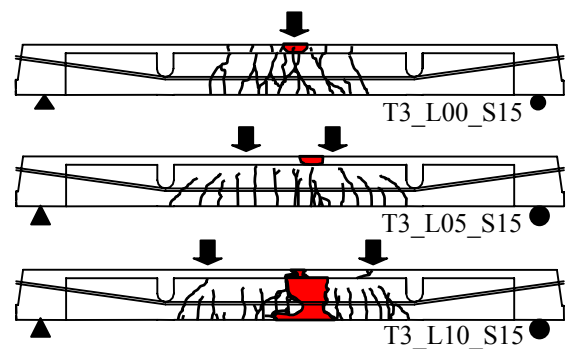
Fig. 5 Crack patterns
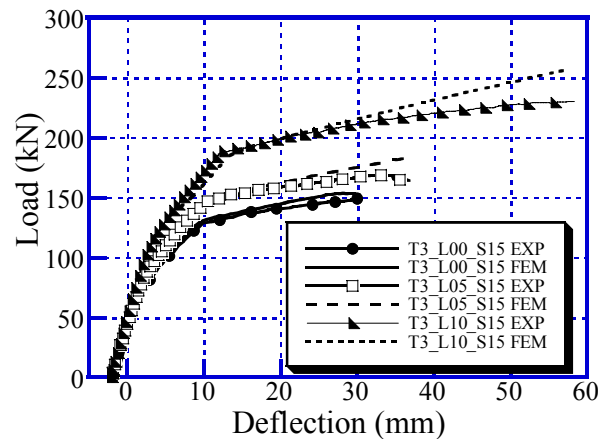
Fig. 6 Comparison of load versus deflection response

Table 3 Summary of measured specimens resistance and deformation

Beams	P_{crack}[*1] [kN]	P_{yield}[*2] [kN]	P_u[*3] [kN]	δ_u[*4] [mm]	d_{pu}[*5] [mm]
T3_L00_S15	72.1	137.2	148.2	30.34	187.3
T3_L05_S15	90.7	146.8	168.4	32.8	186.4
T3_L10_S15	112.3	190.9	230.1	58.3	178.9

*1 Loading resistance at first crack
*2 Loading resistance at yielding of tensile reinforcement
*3 Loading resistance at ultimate stage
*4 Midspan deformation at ultimate stage
*5 Tendon level from extreme compressive fiber to the centroid of tendon at ultimate stage

significant ductility. The second-order effects could also be observed during the test. It is shown that when the loading distance increased, the second-order effects became larger. This indicates that the geometry of loading application has an influence on second-order effects.

4.3 Stress in Tendon at Ultimate

The experimental results of stress increment in tendon of the three beams are summarized in Table 4 and in Fig. 7. Table 4 gives values of the effective prestress of tendon f_{pe} and the tendon stress at ultimate f_{ps}, as measured by the averages of three strain gauges at the midspan cross section of tendons, for all beams. The maximum compressive strain ε_u, measured in the concrete at the upper portion at failure of the beam, and the compressive strength of concrete f_c' are also shown. Figure 7 shows the load versus the stress increase in tendon Δf_{ps} (= f_{ps}-f_{pe}). Before cracking, the stress in tendons showed only a slight increase with the applied load. After cracking, the stress tended to increase significantly at a rate depending on the deformation of a beam. It is interesting to note that the characteristics of load versus stress increment in Fig. 7 express the similar manner with the load versus deflection curve as shown in Fig. 6. Figure 8 shows that the value of stress increase in tendon Δf_{ps} increases in an almost linear manner with the midspan deflection at a similar rate for all beams. With decrease in loading distance L_0, the decrease in both midspan deflection and the stress increment Δf_{ps} at ultimate can be apparently observed in Fig. 6. It is important to note that the stress increment in tendon depends on the geometry of loading application or loading distance, L_a.

4.4 Comparison with Nonlinear FEM Analytical Results

The analytical method presented earlier was used to predict the response of the beams. It is shown in Figs. 6-8 that the analytical and experimental results are in good agreement for load versus deflection, load versus stress increment in tendon and stress increment in tendon versus deflection. This is proven that

the nonlinear FEM analytical model coincides with the response of externally PC beams.

5. COMPARISON WITH THE EXISTING PREDICTION EQUATIONS

As expressed in the previous section, the numerical solution techniques can be used to predict the tendon stress. However, a simplified method is needed for the design code purposes. This paper shows the accuracy in prediction of the existing design codes with the presented experimental results.

Thus, in this study, existing prediction equations, as well as ACI 318-99 code and AASHTO LRFD code were examined.

Table 4 Summary of experimental results

Beams	UNIT: N/mm^2				×10^{-6}
	f_c'	f_{pe}	f_{ps}	Δf_{ps}	ε_u
T3_L00_S15	61.4	956.9	1239.8	282.9	3400
T3_L05_S15	62.3	918.7	1237.1	318.4	2700
T3_L10_S15	56.4	913.5	1451.1	537.6	2900
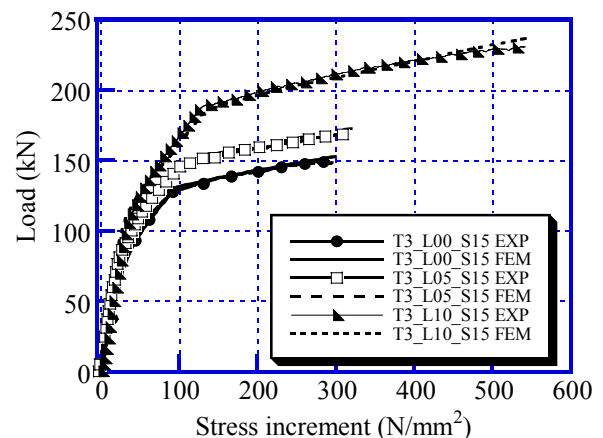
Fig. 7 Load versus stress increase in tendon
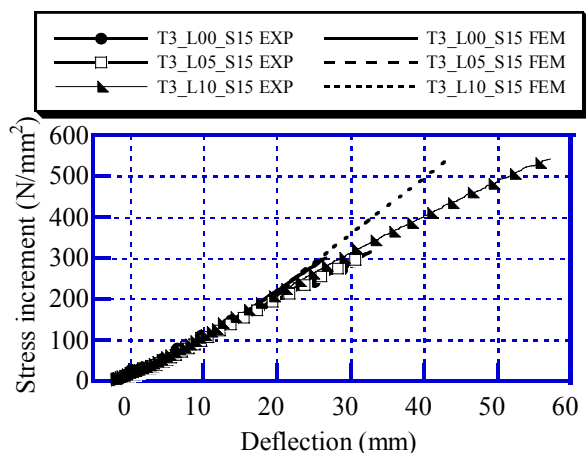
Fig. 8 Relationship between stress increment and deflection of beams

The ACI Code equation is written as:

$$f_{ps} = f_{pe} + 70 + \frac{f_c'}{k\rho_p} \leq f_{pe} + C \qquad (1)$$

when, $L/d_{ps} \leq 35$: k = 100 and C = 420

$L/d_{ps} > 35$: k = 300 and C = 200

where, L is the span length and d_{ps} is the effective depth of external tendon.

AASHTO LRFD Bridge Design recommends a stress in unbonded tendons of flexural members in term of bond reduction factor Ω_u. It can be obtained from the following expression:

$$f_{ps} = f_{pe} + \Omega_u \cdot E_{ps} \cdot \varepsilon_{cu}\left(\frac{d_{ps}}{c} - 1\right) < 0.94 f_{py} \quad (2)$$

where, $\Omega_u = \dfrac{1.5}{\left(L_2/d_{ps}\right)}$ for one-point loading;

$\Omega_u = \dfrac{3}{\left(L_2/d_{ps}\right)}$ for third-point loading

Table 5 and Fig. 9 describe the calculated results of f_{ps} and Δf_{ps} evaluated from ACI 318-99, Eq. (1) and AASHTO, Eq (2). It can be observed that the correlation for Δf_{ps} is quite poor, but their predicting results of Δf_{ps} are generally on the safe side.

Table 5 Calculated results from ACI and AASHTO codes

Beams	UNIT: N/mm²			
	ACI		AASHTO	
	f_{ps}	Δf_{ps}	f_{ps}	Δf_{ps}
T3_L00_S15	1119.6	162.7	1127.7	170.8
T3_L05_S15	1082.8	164.1	1235.3	316.6
T3_L10_S15	1068.7	155.2	1219.5	306.0
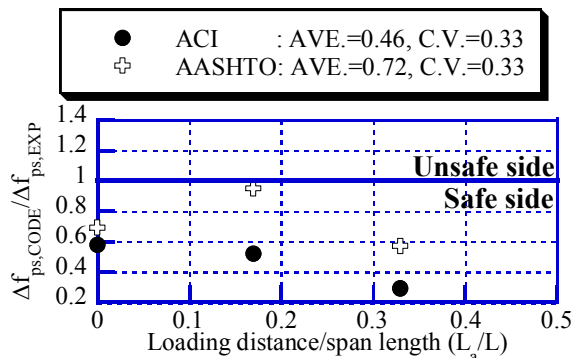
Fig. 9 Comparison in stress increment in tendon between the experimental results and design codes

6. CONCLUSIONS

(1) The geometry of loading application is necessary to consider as a main factor to evaluate the tendon stress at ultimate stage.

(2) The analytical model of nonlinear FEM is applicable to examine the behavior of externally PC beams.

(3) The existing prediction equations cannot determine the stress increment in tendon accurately. The simplified method with higher accuracy is needed for the design purpose by considering the geometry of loading application.

ACKNOWLEDGEMENT

REFERENCES

[1] ACI Committee 318: Building Code Requirement for Reinforced Concrete and Commentary (ACI 318-99/318R-99), American Concrete Institute, Detroit, 1999

[2] AASHTO LRFD: Bridge Design Specifications SI Units First Edition, 1994

[3] JPCEA: Design Specifications for Precast and Externally Prestressed Structures, 1997

[4] Harajli, M.H.: Effect of Span-Depth Ratio on the Ultimate Steel Stress in Unbonded Prestressed Concrete Members, ACI Structural Journal, Vol. 87, No. 3, pp 305-312, 1990

[5] Nakamura, H., Higai, T.: Compressive Fracture Energy and Fracture Zone Length of Concrete, Modeling of Inelastic Behavior of RC Structures under Seismic Loads, ASCE, pp 471-487, 2001

[6] Hordijk, D. A.: Local Approach to Fatigue of Concrete, PhD thesis, Delft University of Technology, 1991